

# Design of the Scramjet Hypersonic Experimental Vehicle

Sara Di Benedetto<sup>1†</sup>, Marco Marini<sup>1</sup>, Pietro Roncioni<sup>1</sup>, Antonio Vitale<sup>1</sup>, P. Vernillo<sup>1</sup>, Salvatore Cardone<sup>2</sup>, Marta Albano<sup>3</sup>, Roberto Bertacin<sup>3</sup>, Enrico Cavallini<sup>3</sup>

*1 CIRA Italian Aerospace Research Centre, 81043 Capua, Italy*

*2 Tecnosistem, 80133 Napoli Italy*

*3 ASI, Agenzia Spaziale Italiana, 00133 Rome, Italy*

[s.dibenedetto@cira.it](mailto:s.dibenedetto@cira.it), [m.marini@cira.it](mailto:m.marini@cira.it), [p.roncioni@cira.it](mailto:p.roncioni@cira.it), [a.vitale@cira.it](mailto:a.vitale@cira.it), [p.vernillo@cira.it](mailto:p.vernillo@cira.it), [scardone@tecnosistemspa.it](mailto:scardone@tecnosistemspa.it), [marta.albano@asi.it](mailto:marta.albano@asi.it), [roberto.bertacin@cira.it](mailto:roberto.bertacin@cira.it), [enrico.cavallini@asi.it](mailto:enrico.cavallini@asi.it)

<sup>†</sup> Corresponding Author

## Abstract

In the frame of the “SPACE-IPERSONICA-TEC” project, funded by the national program PRORA and “Research and Development of a hypersonic demonstrator”, co-funded by the Italian Aerospace Agency (ASI), the Italian Aerospace Research Centre (CIRA) is working at the design of a propelled hypersonic demonstrator, the Scramjet Hypersonic Experimental Vehicle, and its flight experimental mission.

The paper presents the feasibility analysis performed for the definition of the flight mission where different launch scenarios have been considered. The result is an air-launch based on the use of a carrier aircraft and of a launch vehicle capable of guiding the demonstrator to the target altitude and velocity of the flight experiment. Starting from this analysis, the launch vehicle has been preliminarily defined and sized.

At the same time, work has been done on the development of the demonstrator configuration, which takes advantage of the experience and the configuration study carried out in the two EU co-funded projects HEXAFLY [1] and HEXAFLY-INT [2].

A first assumption on the scale of the demonstrator has been done, and its materials layout, its avionics, airframe and the components of propulsive subsystems, including the on-board fuel tanks (hydrogen) for the scramjet engine properly sized, are presented.

Finally, various points along the trajectory have been simulated using CFD for the purpose of verifying the aero-propulsive balance and defining the aerothermal loads and aerodynamic coefficients which will be used for the flight mechanics analysis and trajectory calculation, and for the thermal analysis.

The previous points have allowed for the definition and assessment of a first set of system and mission requirements.

## 1. Introduction

The research and experimentation for hypersonic flight, aimed at creating and testing the enabling technologies for future high-speed systems, is one of the main research topics on which CIRA has been engaged for over 15 years, mainly with the participation on the various EU projects dedicated to hypersonic flight for passenger transport (LAPCAT I&II [3], ATLLAS I&II [4], FAST20XX [5], HEXAFLY [1], HEXAFLY-INT [2], STRATOFly RD[7]), but also with military and civil national projects.

In 2021 CIRA, thanks to the “SPACE-IPERSONICA-TEC” project, funded by the national program PRORA, and taking advantage from its strong involvement in the European projects just mentioned, and in particular in HEXAFLY-INT (flight test of an unpropelled vehicle for hypersonic flight), and previously in HEXAFLY, posed the challenge of designing a scramjet hypersonic demonstrator for a future test in-flight.

In 2022, as the project was of high interest also of the Italian Space Agency, the two national entities decided to co-fund the research activities by a dedicated agreement “Research and Development of a hypersonic demonstrator”, which has the aim at completing the project Preliminary Design Review by 2025.

The main project objectives, then translated into requirements during the project development, have been defined considering also the international scenario of propelled hypersonic aircraft, analysed from the sixties to today, ranging from American experimental vehicles (X-15A, X-43A, X-51A), which have actually flown, to experimental vehicles in national or international cooperation in recent years, such as the Brazilian I4-X, the Franco-Russian project LEA and the project funded by the European Commission HEXAFLY. The research criterion was to select only propelled

hypersonic vehicle demonstrators designed to create and test the enabling technologies for future hypersonic civil transport systems, thus leading to the following system and mission objectives:

- Aircraft class: length 3÷8 m, mass 600÷2000 kg
- Hypersonic flight at Mach=6÷8, constant altitude 27÷32 km, stable and trimmed
- Aero-propulsive balance with an aerodynamic efficiency  $L/D=3÷4$
- Scramjet propulsion system with hydrogen fuel, running steadily for at least 10 seconds.

This paper deals with the starting activities performed at system level for the system and mission definition.

The approach defined is based on the tight interaction between subsystems up to the completion of system and mission design, as described in the flow chart below (see Figure 1). The process is coordinated by the system, which represents the design authority, to fulfil the mission and system requirements defined from the mission objectives.

The flow chart clarifies how, in the multidisciplinary approach, each discipline interacts with the other ones and with the system, and which parameters are being exchanged.

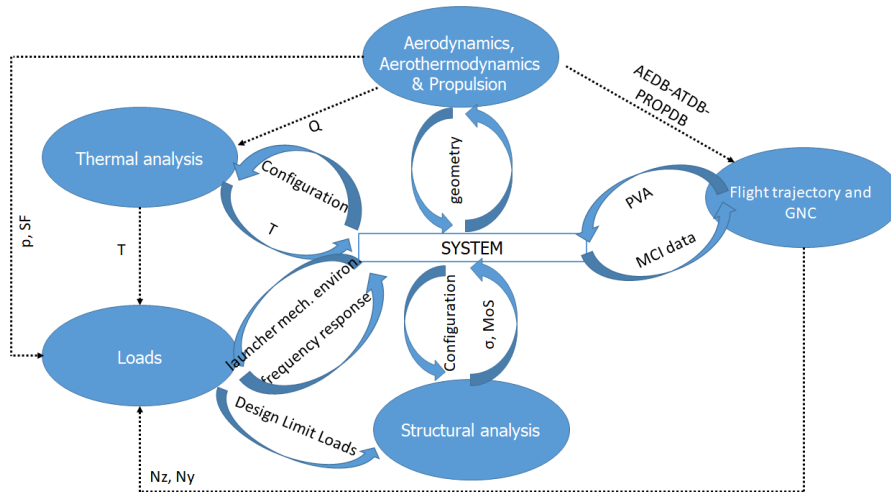


Figure 1: Multidisciplinary interactions and interdependencies within the different disciplines

## 2. The Hypersonic Flight Demonstrator

The configuration of the Scramjet Hypersonic Experimental Vehicle (SHEV) is based on the concept of "waverider", i.e., a hypersonic vehicle with high aerodynamic efficiency in supersonic regime obtained through the exploitation of the shock waves that form on the load-bearing surfaces, a phenomenon known as "compression lift".

The demonstrator must also include a scramjet air-breathing propulsion system

For this concept, in particular, the configuration studied in the EU-FP7 HEXAFLY project [1] and illustrated in Figure 2 was considered:

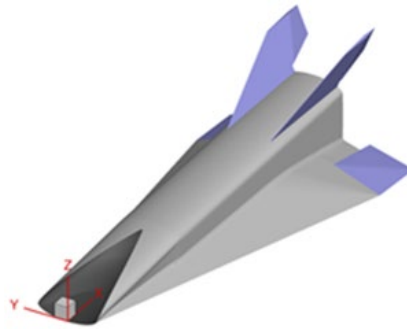


Figure 2: Configuration of the HEXAFLY project demonstrator.

This configuration has been modified to meet the project requirements; in particular:

1. the configuration has been scaled up by a scale factor of 1.43 applied homothetically to to simplify the housing of the on-board equipment and to solve some structural criticalities faced in HEXAFLY-INT (heat fluxes reduction needed in some critical regions);
2. The sharp edges have been replaced with suitable rounding;
3. The on-board equipment has been defined and preliminary installed;

4. The internal structure has been defined and a preliminary assumption on the materials layout has been made on the base of the first thermal analyses.

To develop the point 1, and in particular to fix a range for the mass of the demonstrator, both quadratic and cubic scaling laws have been applied (Figure 3), providing the following data for length and mass:

- L=4.5 m, W=1.76 m
- Mass 920÷1200 kg

The final result is shown in Figure 4.

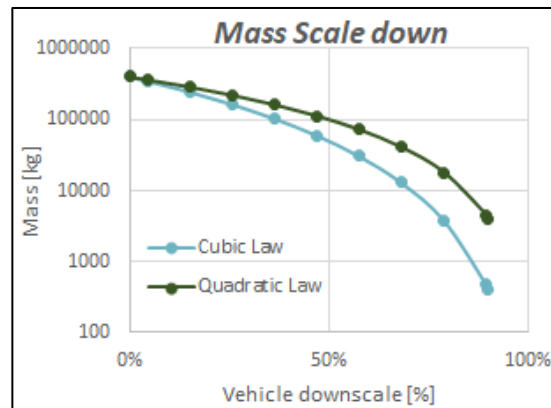


Figure 3: Scaling of the demonstrator; comparison between cubic and quadratic law

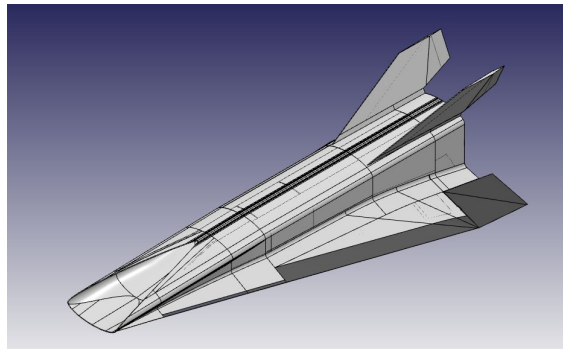


Figure 4: SHEV external configuration

The demonstrator is equipped with its own avionic and in-flight measurement system; Figure 5 represents the block diagram of the preliminary design of the avionic system, based on the main following subsystems: Power Management System (PMS), Flight Control Computer (FCC), In-flight measurement system (IFMS), servo-actuator and Pyro Control (ACU, PYRO), Telemetry and Telecommand (TM/TC), Scramjet Control Unit.

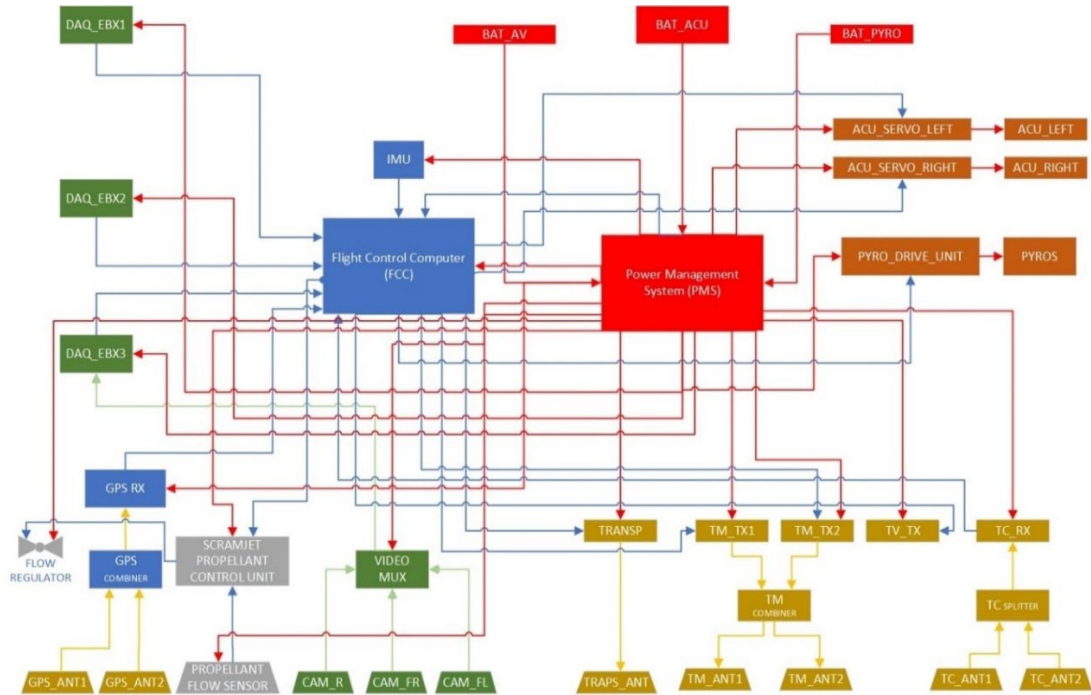


Figure 5. Avionic System Block Diagram

### 3. Mission Scenario

The preliminary mission concept envisages an air-launched solution with a carrier (stage I) capable of releasing the payload, composed by the hypersonic demonstrator and a launch vehicle equipped with a booster, at a target point in terms of speed and altitude, preliminary assumed as (Table 3):

Altitude	13.5÷15 km
Mach number	0.6

Table 1. Release conditions of the payload from carrier aircraft

From here the launch vehicle accelerates until it reaches the foreseen trajectory target point (experimental window) where the hypersonic propelled demonstrator is separated from the launch vehicle and the scramjet starts working, as described in following schedule of mission events and macro-phases:

Table 2. Events and phases of the experimental mission

Table 2. Events and phases of the experimental mission		
1	Take-off of carrier aircraft from a civil or military airport	<b>Phase -1</b>
2	Subsonic flight towards the (segregated) flight testing area	
3	Acceleration to payload release conditions (Mach=0.6)	
4	Separation of payload (Launch Vehicle+Demonstrator) from carrier aircraft and ignition of Launch Vehicle's booster (sep1)	<b>Phase 0</b>
5	Acceleration from separation Mach number (0.6) up to target Mach number (7.35) and altitude (27 km) with aerodynamically controlled Launch Vehicle	
6	Launch Vehicle's booster burn-out and optimization of separation conditions	
7	Separation of hypersonic propelled demonstrator from the launch vehicle (sep2)	
8	Ignition and tuning of the scramjet engine in the experimental window (steady function for at least 10 seconds)	<b>Phase 1</b>
9	Scramjet engine shutdown	<b>Phase 2</b>
10	Gliding decelerating phase (aerodynamic control down to Mach=2) of the hypersonic propelled demonstrator	
11	Loss of control, Splash Down	

Figure 6 shows a graphical representation of the experimental flight mission (top) and a detail of the mission key events (bottom).

Note that it is assumed that the carrier aircraft returns back and lands at the airport, whilst both the launch vehicle and the hypersonic propelled demonstrator are disposable vehicles, thus they are not recovered.

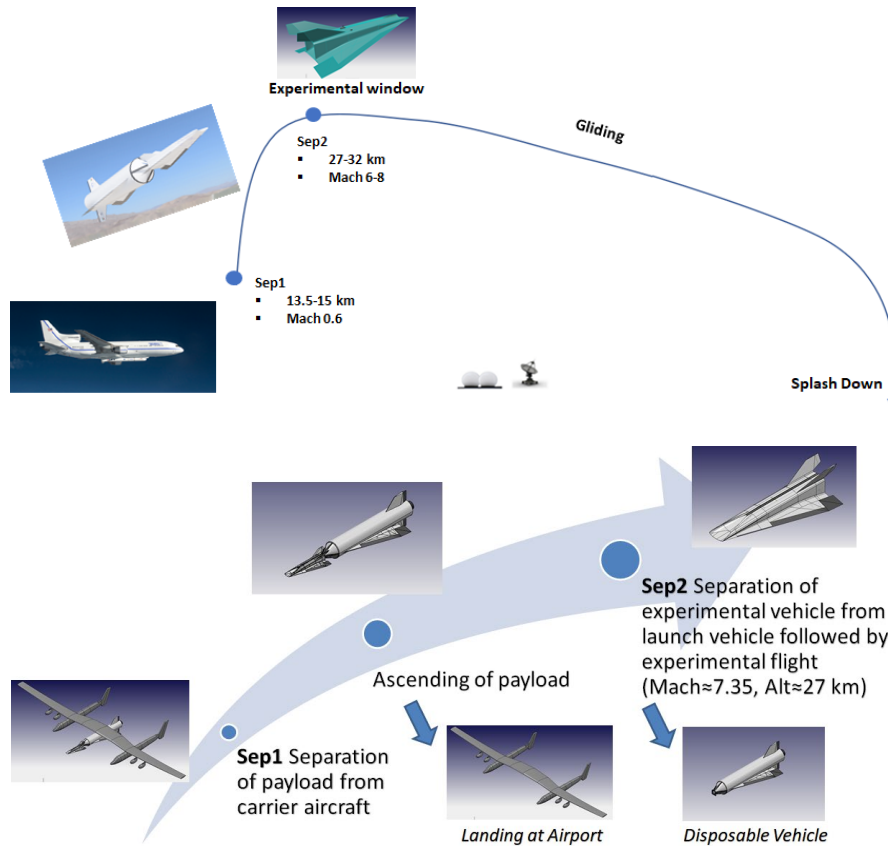


Figure 6. Graphical representation of the experimental mission (top) and key events (bottom)

The point-by-point preliminary (nominal) mission profile from sep1 to end of mission is shown in Figure 7, in terms of properties as function of time, highlighting in particular the experimental window with the scramjet propulsive system on (steady functioning for at least 10 seconds) and the main mission parameters to be achieved, i.e., Mach number and altitude (and initial velocity), also with a preliminary indication of demonstrator's mission global loads:

- Mechanical load → maximum dynamic pressure  $P_{dyn}=71.7$  kPa
- Inertial load → maximum acceleration  $a/g=2.8$
- Thermal load → maximum stagnation-point heat flux  $q_{sp}=640$  kW/m<sup>2</sup> and stagnation-point thermal load 96.62 MJ/m<sup>2</sup> (hypothesis of emissivity coefficient  $\epsilon=0.4$ )

A deeper flight mechanics analysis is presented in section 5.

### 3.1. The Launch Vehicle

The Launch Vehicle (LV) has been preliminarily defined, mainly in terms of solid booster (SRM) needed to match the mission objectives, of external configuration (a wing body with elevons and vertical tails) and of mechanical interface with the hypersonic propelled demonstrator SHEV.

The Launch Vehicle connected to the hypersonic propelled demonstrator is shown in Figure 8, where also details of vertical tail and mechanical interface to hypersonic propelled demonstrator are illustrated.

This preliminary concept is currently under a deeper definition phase and related verifications (aero-propulsive, structures and materials, mass, centre of gravity and inertia moments, flight mechanics, aerodynamic controls, avionics, mechanisms and actuators, etc.), in such a way to deliver soon the final configuration.

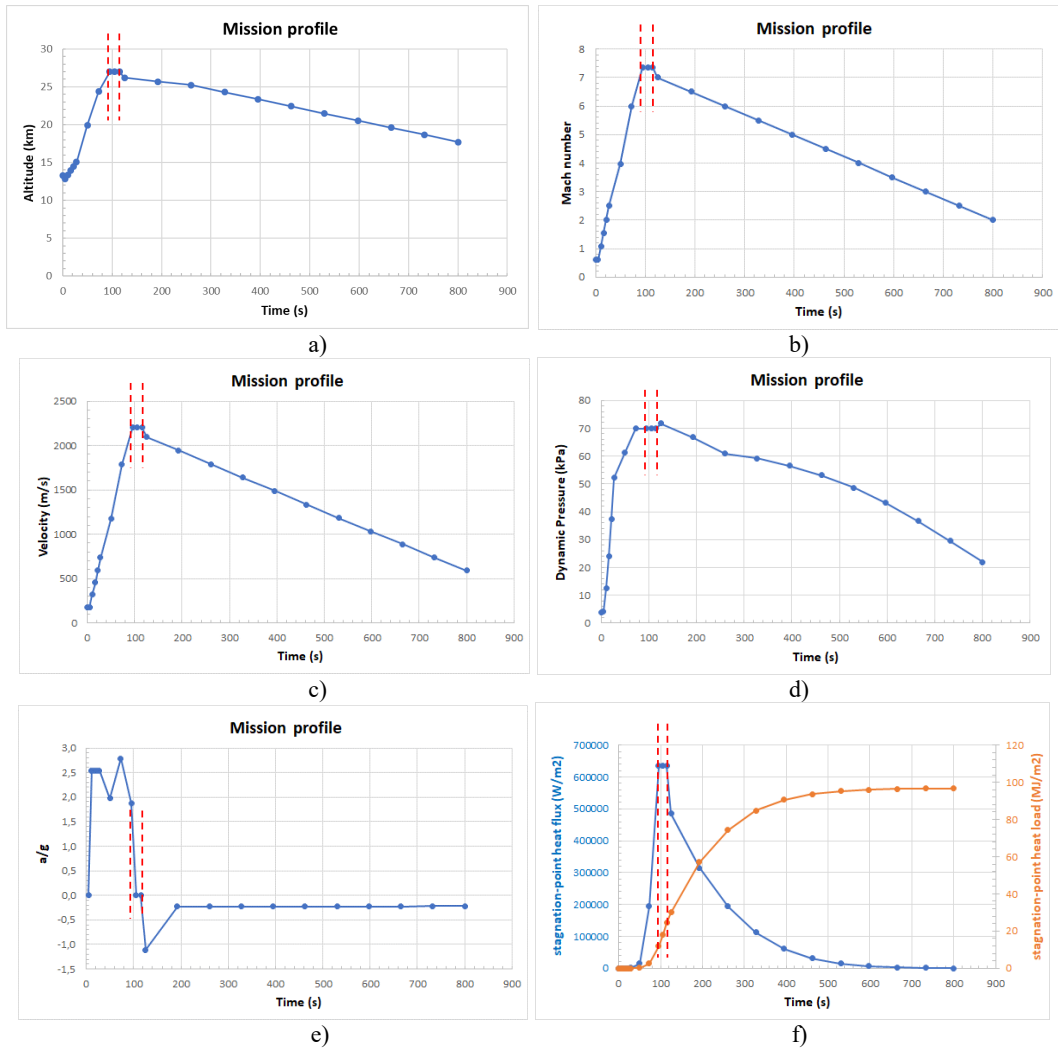


Figure 7. Preliminary mission profile: a) altitude; b) Mach number; c) velocity; d) dynamic pressure; e) acceleration; f) aerothermal loads

Table 3 reports the preliminary dimensions and masses of the launch vehicle (LV) preliminarily and of the hypersonic propelled demonstrator (SHEV), which together constitute the payload of the launch system.

Table 3. Dimensions (above) and masses (below) of the payload, i.e., the launch vehicle connected to the hypersonic propelled demonstrator

Total length of launch system	14.3 m
Length of launch vehicle (including nozzle and I/F)	10.2 m
Wingspan of launch vehicle	3.5 m
Maximum height of launch vehicle	3.5 m
Fuselage diameter of launch vehicle	1.5 m
Reference surface of launch vehicle	21.05 m <sup>2</sup>
Length of hypersonic propelled demonstrator	4.5 m
Wingspan of hypersonic propelled demonstrator	1.76 m
Reference surface of hypersonic propelled demonstrator	4.8 m <sup>2</sup>

Initial mass of launch system	14120 kg
Mass of hypersonic propelled demonstrator	1120 kg
Initial mass of launch vehicle	13000 kg
Mass of solid grain SRM	3025 kg
Dry mass of launch vehicle	9975 kg

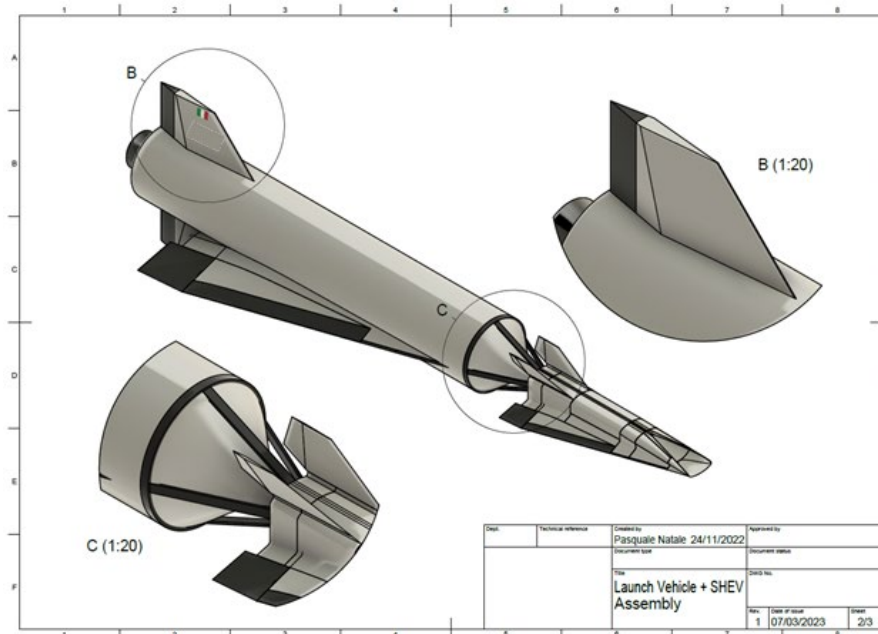


Figure 8. Launch Vehicle with details of vertical tail and mechanical interface to hypersonic propelled demonstrator

A particular attention is currently being given to the definition of the interface between the launch vehicle (LV) and the hypersonic propelled demonstrator (SHEV), whose main functions are:

- Thermo-structural resistance along the entire ascent trajectory of launch system, from sep1 to sep2 (see Table 2);
- Proper massflow accommodation through the propulsive duct of SHEV, by avoiding any shock wave and/or flow instability (minimum drag axial-symmetric shape);
- Separation of SHEV by avoiding any mechanical interference/shock between LV and SHEV.

The solution currently under elaboration is depicted in Figure 9:

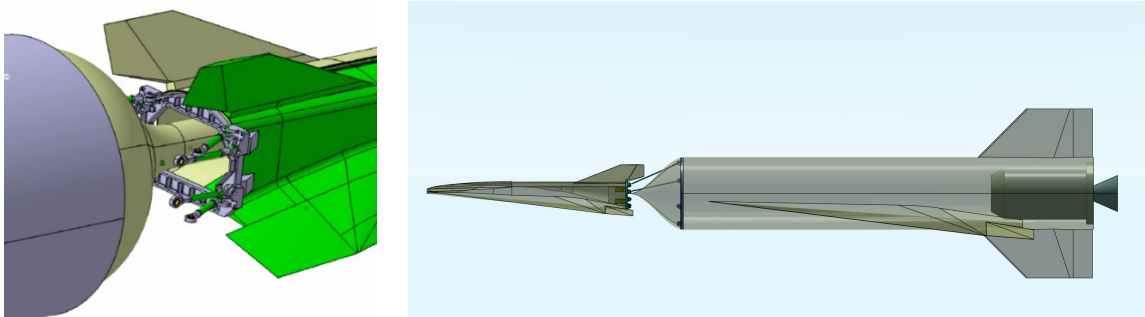


Figure 9. Mechanical interface and shaped cone connecting the launch vehicle and the hypersonic propelled demonstrator

For what concerns the LV structure it is mainly composed by the following major items: fuselage, wings, wing leading edges, elevons and vertical fins.

The fuselage structure (see Figure 10) is realized with a build-up approach; it is composed by three main sections, i.e., forward fuselage, central fuselage, rearward fuselage and tail fuselage. As a first structural element hypothesis, the structure of fuselage is mainly composed by Double T frames, Z shape stringers and panels. All these components are realized by milling metallic billets, the panels are realized in composite material.

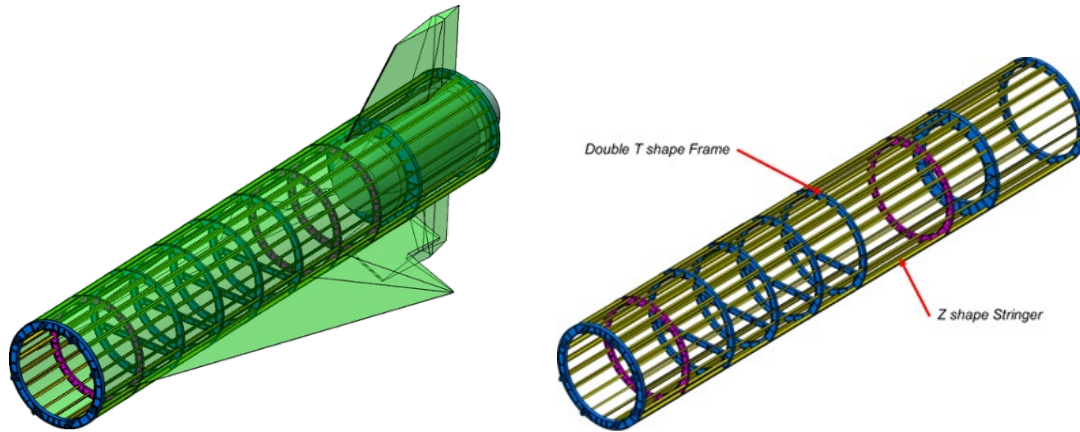


Figure 10. Launch Vehicle Fuselage Structure

#### 4. AEDB Characterization

The Aerodynamic Data Base (AEDB) Building is the overall procedure that allows to obtain a full and integral set of information and/or data that characterize the aerodynamic environment in terms of flow field features, global and local forces, pressure distributions and thermal loads over the vehicle surfaces.

These data are inputs for several disciplines as flight mechanics, thermo-structural analysis, but also in some cases for propulsive database building. In this section the starting CFD simulations concerning the aero-propulsive balance and the aerodynamic database building are reported.

##### 4.1 Aero-Propulsive Balance and Aerodynamic Efficiency

The verification of the aeropropulsive balance and aerodynamic efficiency in cruise conditions is conducted at two flight conditions (see Table 4).

Table 4: Matrix test for hypersonic cruise conditions

Altitude	H = 27 km	H = 31.9 km
Static pressure $p_\infty$	1828 Pa	875.5 Pa
Static temperature $T_\infty$	222.3 K	235.97 K
Static density $\rho_\infty$	0.02852 kg/m <sup>3</sup>	0.01293 kg/m <sup>3</sup>
Mach number $M_\infty$	7.350	7.355
Flow velocity $u_\infty$	2202 m/s	2264.7 m/s
<b>MFR</b>	<b>4.851 kg/s</b>	<b>2.246 kg/s</b>

Numerical CFD viscous simulations were conducted with the ANSYS FLUENT® CFD code on a grid of 7.6 million cells (Figure 11).

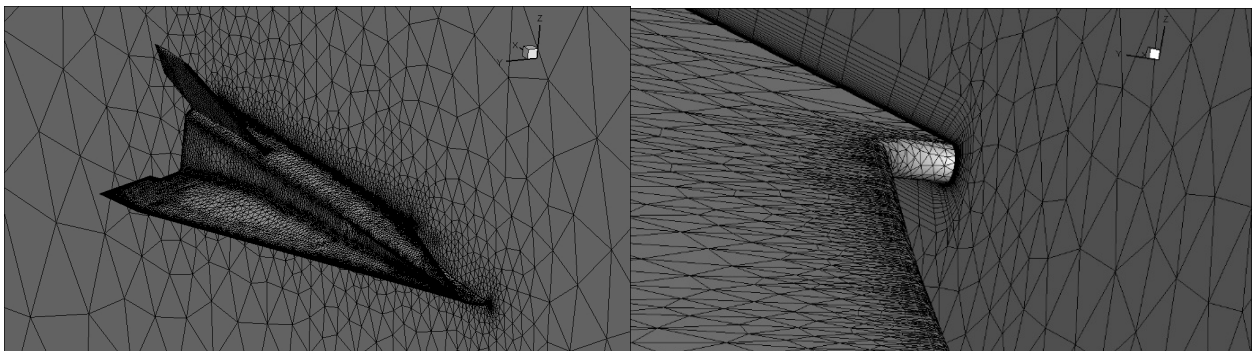


Figure 11: Calculation grid for simulations with the engine on.

Table 5 summarizes the aerodynamic parameters of interest. The values were extracted by distinguishing the external part (fuselage, wings and empennages) and the internal part composed of air intake, combustor and nozzle. The flight

experiment takes place in motor-on conditions, and in these conditions for the purposes of aerodynamic efficiency only the external part of the aircraft is considered. From the table you can see how the efficiency  $E_{\text{ext}}$  (external) is well above 4 (almost 5). In addition, from the table it is possible to see that even the total efficiency  $E_{\text{tot}}$ , which makes sense as argued above for the motor-off conditions that occur after the shutdown of the scramjet, is well within the mission requirements (value around 3.5).

Table 5: Summary of aerodynamic parameters of cruising with the engine off

H	Mach	Type	CL_ext	CL_int	CL_tot	CD_ext	CD_int	CD_tot	CM_ext	CM_int	CM_tot	E_ext	E_int	E_tot
27.00	7.350	No-Inj	0.04004	0.001299	0.041339	0.008267	0.00336	0.01163	-0.02362	-0.00304	-0.02667	4.8431	0.3865	3.5552
31.90	7.355	No-Inj	0.03996	0.001166	0.041130	0.008604	0.00345	0.01205	-0.02355	-0.00296	-0.0265	4.6449	0.3380	3.4125

Following the verification of the aerodynamic efficiency requirement, it was then necessary to verify the aeropropulsive balance. This expression means that the thrust delivered by the scramjet engine must be verified to counterbalance the aerodynamic drag of the external part of the aircraft. The net thrust, i.e. the gross thrust decreased by the drag of the air intake (which is considered to be part of the engine), must therefore be greater than or equal to the external drag.

Simulations with air-hydrogen reacting flow were therefore conducted under the same asymptotic conditions as in Table 4. In order not to weigh down the numerical calculations too much, a single-step chemical scheme for modelling air-hydrogen combustion was used that considers the only reaction between oxygen and hydrogen, with nitrogen that remains inert and unchanged along the entire internal duct.

Table 6 shows the main results in terms of axial forces for both motor-off and motor-on conditions. First of all, it can be noted that the aero-propulsive balance requirement is met at both altitudes. In fact, the total force resistance (external + internal) is negative, which means that the thrust of the scramjet engine ( $\text{Thrust} > \text{Drag}$ ) is higher than the external resistance.

Table 6: Summary of axial forces acting on the hypersonic propelled demonstrator.

		Ext	Int	Tot
<b>Forces (N)</b>	<b>27 km</b>	<b>2820</b>	<b>-3032</b>	<b>-213</b>
<b>Mot-on</b>	<b>31.9 km</b>	<b>1357</b>	<b>-1380</b>	<b>-23</b>
<b>Forces (N)</b>	<b>27 km</b>	<b>2740</b>	<b>1113</b>	<b>3853</b>
<b>Mot-off</b>	<b>31.9 km</b>	<b>1367</b>	<b>548</b>	<b>1915</b>

## 4.2 Aerodynamic Database

The aerodynamic database is provided as a function of Mach number ( $M_\infty$ ), angle of attack ( $\alpha$ ) and the elevon deflections ( $\delta_e$ ) in *fuel-off* conditions. However, the analysis does not consider the effect of sideslip angle ( $\beta$ ). The reference quantities are reported in Table 7. The Centre of Gravity is located at  $x_{\text{CoG}} = 2.33$  m from the nose.

Table 7: Summary: Reference Quantities

Reference Length ( $L_{\text{ref}}$ )	4.1248 m
Reference Surface ( $S_{\text{ref}}$ )	4.7936 m <sup>2</sup>
Mass	1120 kg
$x_{\text{CoG}}$ range	2.30- 2.33 m

The aerodatabase of the SHEV vehicle has been completed for all the mission that foresees, after the ignition time (at least 10 seconds at constant altitude), a gliding aerodynamically controlled phase from Mach 7.35 to Mach 2.0, followed by a splash down on the sea. The CFD computations have been obtained running on the same grid of 7.6 million of cells and with the same turbulence model, but now in fuel-off conditions (see Table 8).

A sensitivity in fuel-on cruising conditions has been also performed by adding  $\pm 2$ deg to  $\text{AoA} = 0$  deg at  $M = 7.35$  while a range from  $-4^\circ$  to  $+4^\circ$  for the AoA in fuel-off ones has been considered. The fuel-off descent, based on the estimated preliminary trajectory, needs to be verified downstream in the analysis of Flight-Mechanics. The AEDB data is released with increasing reliability for flight mechanics analysis and trajectory calculation in the framework of the project.

Table 8: Test Matrix for CFD computations

h (km)	Mach	AoA	engine	P	Temp	Dens	a	Vel	mu
27.00	7.35	-2, 0, 2, 4	fuel-off/on	1847.46	223.65	0.028777	299.799	2203.52	1.47164E-05
26.19	7	-2, 0, 2, 4	fuel-off	2091.26	222.84	0.032693	299.255	2094.79	1.46711E-05
25.25	6	-2, 0, 2, 4	fuel-off	2416.16	221.90	0.037932	298.623	1791.74	1.46324E-05
23.36	5	-2, 0, 2, 4	fuel-off	3236.22	220.01	0.051243	297.349	1486.75	1.45123E-05
20.54	3.5	-2, 0, 2, 4	fuel-off	5028.52	217.19	0.080656	295.437	1034.03	1.43532E-05
17.72	2	-2, 0, 2, 4	fuel-off	7843.63	216.65	0.126124	295.070	590.14	1.43226E-05

Looking at the following figures (from Figure 13 to Figure 15) we can deduce that:

- Linear trend of CL for full vehicle (External + Internal) except in fuel-on (M=7.35) where there is a decrease of the derivative  $CL_\alpha$  with increasing of AoA.
- Quadratic trend of CD. At M=7.35 fuel-on the aero-propulsive balance is “negative” at AoA=2° that means that the external drag is greater than the “net thrust” of the internal flow path. This is due to the fact that at higher angle of attack the intake captures less air and so the scramjet engine gives a lower “thrust”. The opposite can be observed at AoA=-2° where there is a higher mass flow rate and thrust.
- In the gliding phase from M=7.35 to M=2.00 an out of trend of CL can be observed (see Figure 15). At M=3.5 the CL is lower than expected. This is due to the expulsion of the shock waves train from combustor duct, and the consequent positioning of the shock wave over the intake giving a local down-lift.
- The external coefficients are all regular as expected from linear aerodynamics. There is no influence of the shock wave train positioning along the gliding trajectory.
- From the internal coefficients we can see, as expected from previous considerations, great values of drag and down-lift at M=2.00, 3.50 (expulsion of shock waves train), small values for other Mach number and in particular negative drag (that means positive internal thrust) at M=7.35 Fuel-On.

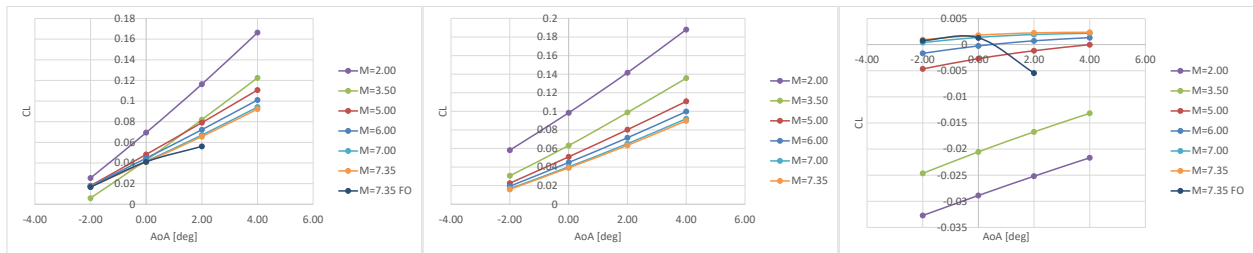


Figure 12: Lift Coefficient: Full vehicle, External part, Internal part.

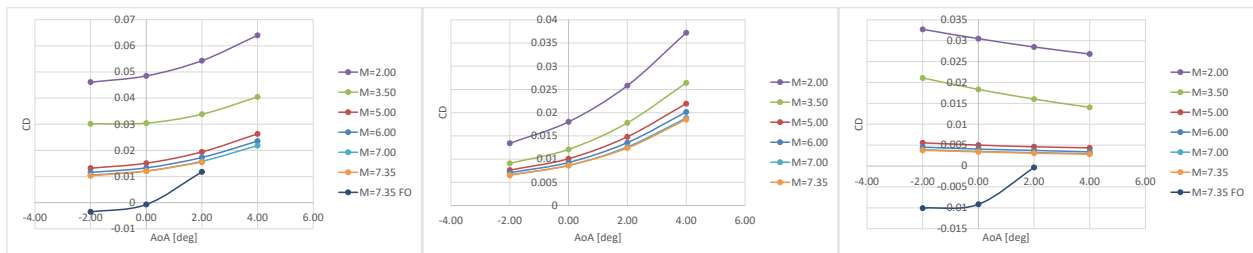


Figure 13: Drag Coefficient: Full vehicle, External part, Internal part.

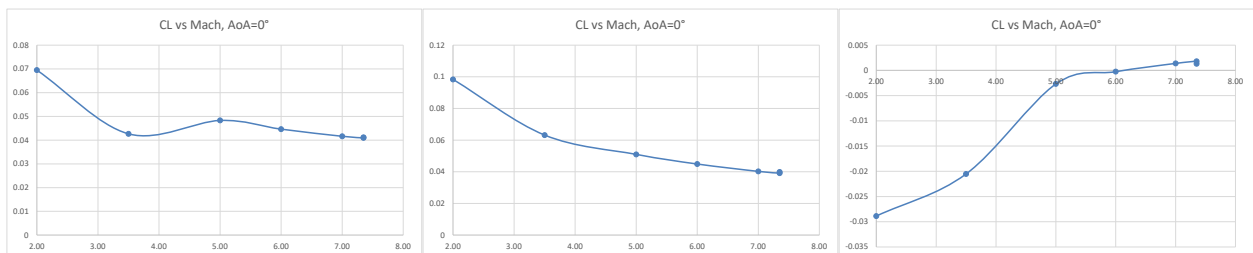


Figure 14: Lift Coefficient at AoA=0°: Full vehicle, External part, Internal part.

The variation of the aerodynamic coefficients due to the control surfaces is assessed as the difference between the aerodynamic coefficients of the configuration evaluated with deflected elevon and the coefficients evaluated with the

undeflected elevon (e.g.,  $\Delta C_M(\delta_e) = C_{M\delta_e} - C_{M\delta_e=0}$ ) on a simplified configuration constituted of the wing and elevon.

Figure 16, Figure 17 and Figure 18 show, respectively, the lift, drag and pitching moment coefficient distributions in function of AoA for three different elevon deflections (from  $-20^\circ$ ,  $-5^\circ$ ,  $+10^\circ$ ) and Mach numbers (from 2.0 to 7.35). Please, note that the pitching moment is evaluated with respect to  $X_{CoG}=2.3099$  m.

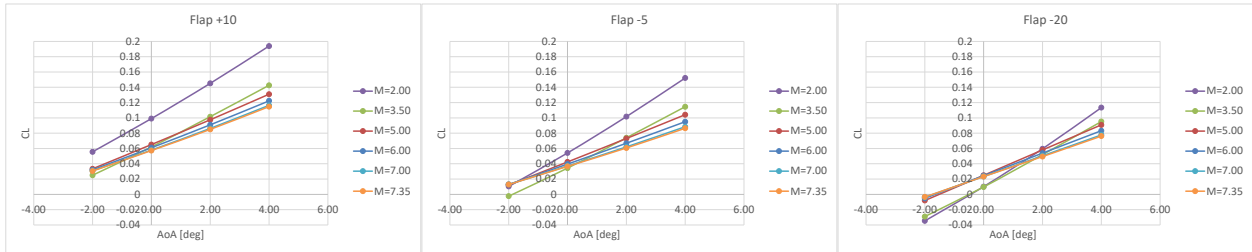


Figure 15: Lift Coefficient at three different elevon deflections.

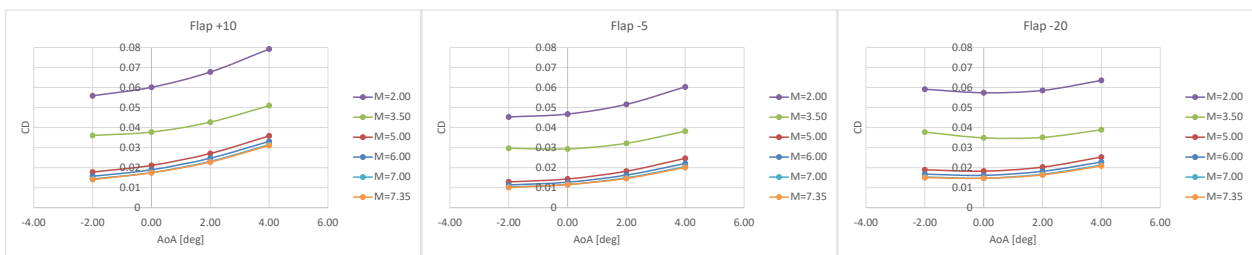


Figure 16: Drag Coefficient at three different elevon deflections.

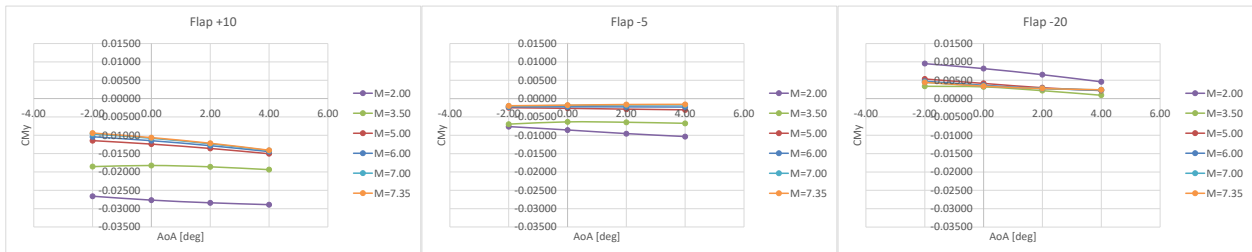


Figure 17: Pitching Moment Coefficient at three different elevon deflections.

## 5. Flight Mechanics Analyses

### 5.1 Analyses definition

The flight mechanics analyses aim to assess the feasibility of the mission and to provide useful information to the system integrators about the vehicle configuration. The analyses are carried out using a preliminary version of the AEDB, which was available when the analyses started. Phase 1 and phase 2 of the mission profile are only examined and the mission is assumed purely longitudinal. Figure 1 shows the flight mechanics analyses activity flow.

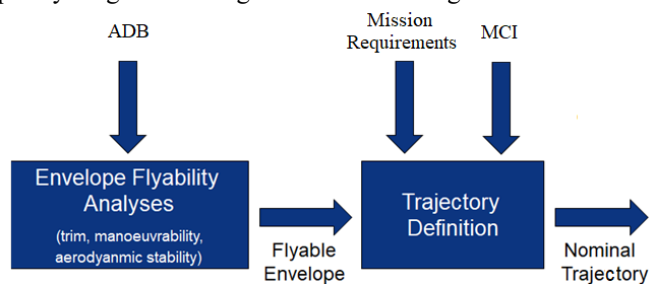


Figure 18: Flight mechanics analyses activity flow

The first set of analyses, denoted as envelope flyability analyses, assess the properties of the vehicle on the whole flight envelope of interest, defined in the Mach–angle of attack plane. These properties include:

- Trim: computation of the flap deflection ( $\delta_{trim}$ ), if it exists within the allowable deflection range, which makes null the pitching moment coefficient.
- Maneuverability: in each flight envelope point in which the vehicle is trimmable, check if the flap deflection required for trim is within its allowable range reduced by a margin  $G_{man}$ , denoted as maneuverability margin and usually assumed equal to 20%.
- Static stability: in each flight envelope point in which the vehicle is trimmable, check if a perturbation of the angle of attack produces a variation of the pitching moment coefficient that opposes to the perturbation.

It is worthy to remark that the results of the above listed analyses depend on the position of the vehicle's centre of gravity (CoG). For this reason, a sensitivity analysis of the flying qualities with respect to the CoG position is carried out and the position that guarantees the best flyability characteristics is identified.

Next to the flyability analyses, the trajectory definition is performed by computing the time histories of position and velocity of the vehicle centre of gravity, and of all the derived parameters that are relevant for mission. This task requires the definition of the vehicle guidance laws, which for the considered mission, consist of the computation of the angle of attack profile. To this aim the following nonlinear constrained optimization problem shall be solved:

$$\begin{aligned}
 & \min_{\alpha} J \\
 \text{s. t. } & \begin{cases} \dot{x}(t) = F(\alpha(t), x(t), t) \\ B(\alpha(t), x(t), t) = 0 \\ C(\alpha(t), x(t), t) \leq 0 \\ \alpha_{min} \leq \alpha \leq \alpha_{max} \end{cases}
 \end{aligned}$$

where  $\alpha$  is the angle of attack, which shall vary in a predefined range;  $x$  is the state vector of the vehicle;  $t$  is the time;  $J$  is the objective function, which is defined as the difference between the obtained trajectory altitude and the altitude mission profile presented in section 2;  $F$ ,  $B$ , and  $C$  are functions which represent the equations of the vehicle's translational dynamics, and the mission and system requirements. The optimization problem is solved numerically and independently for each of the two examined mission phases.

## 5.2 Analyses results

Figure 20 and Figure 21 show the flyability analyses results for motor off and motor on, respectively, on the whole flight envelope of interest and for CoG placed at 56% of the aerodynamic reference length, which is the best position identified through the sensitivity analysis. For motor off, the vehicle is always trimmable, except for a small region of the envelope at high angle of attack (bigger than 2 degrees) and Mach number between 3 and 4.5. The required trim deflection is always negative (that is, in the upper direction), as expected for this type of vehicle. Maneuverability is guaranteed in the whole trimmable region with a margin of 10%, which increases to 20% if Mach number is lower than 3 or bigger than 4. The vehicle is always stable except for high Mach number (bigger than 6) at positive angle of attack; however, a stable corridor at low angle of attack is available. For motor on, only one value of Mach number is examined, that is 7.35, assumed as nominal condition during the experimental window. In this condition the vehicle is trimmable for angle of attack lower than 1.5 degrees and the trim conditions are always stable. The static margin, presented in Figure 21, represents an indicator of the static stability. Indeed, it defines the allowed rearward shift from the current CoG position beyond which the vehicle becomes unstable. It values few percentual points for negative angle of attack (as typical for hypersonic vehicle) and increases significantly when the angle of attack is positive. These results point out that the vehicle has good properties, if the position of the CoG is properly chosen.

Figure 22 and Figure 23 present the outcomes of trajectory definition analysis. The nominal trajectory is plotted on the stability map in the Mach-angle of attack plane, and the most significant trajectory parameters are plotted against the constraints imposed by mission and system requirements. The figures highlight that:

- when motor is on, the value of the angle of attack is constant and equal to -1.05 degrees, which guarantees an aerodynamic efficiency bigger than 3 (as requested by mission requirements);
- when motor is off, the vehicle is always within the trimmable and static stable corridor;
- requirements concerning mechanical load, inertial load, and thermal load are always satisfied.

These results, although obtained using a preliminary version of the AEDB, confirm the feasibility of the mission.

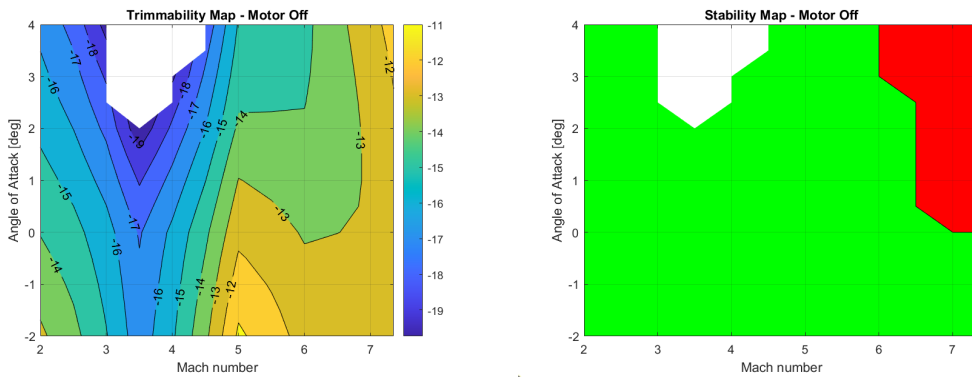


Figure 19: Flyability results for motor off: trim (left) and static stability (right)

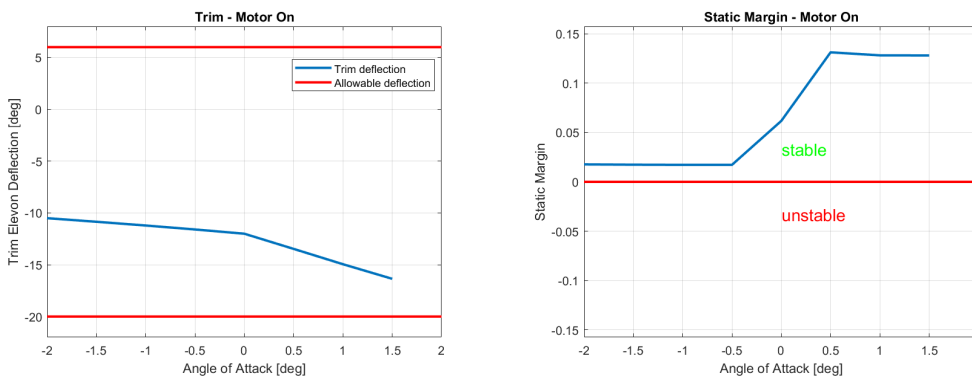


Figure 20: Flyability results for motor on: trim (left) and static margin (right)

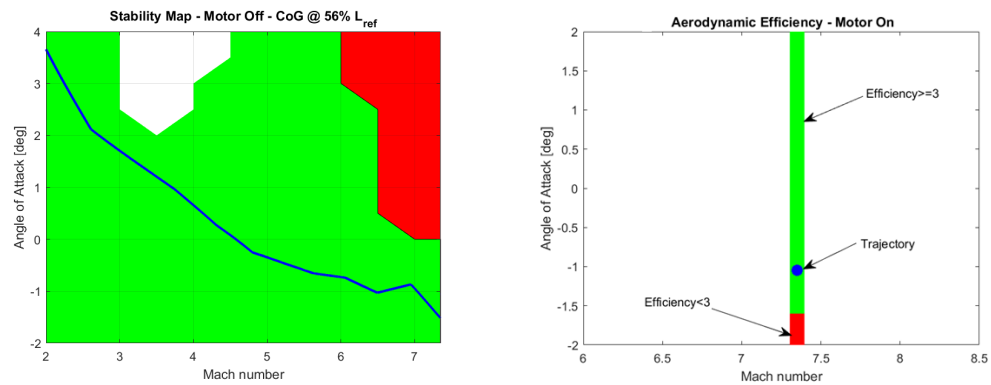


Figure 21: Nominal trajectory (blue) on the stability map: motor off (left) and motor on (right)

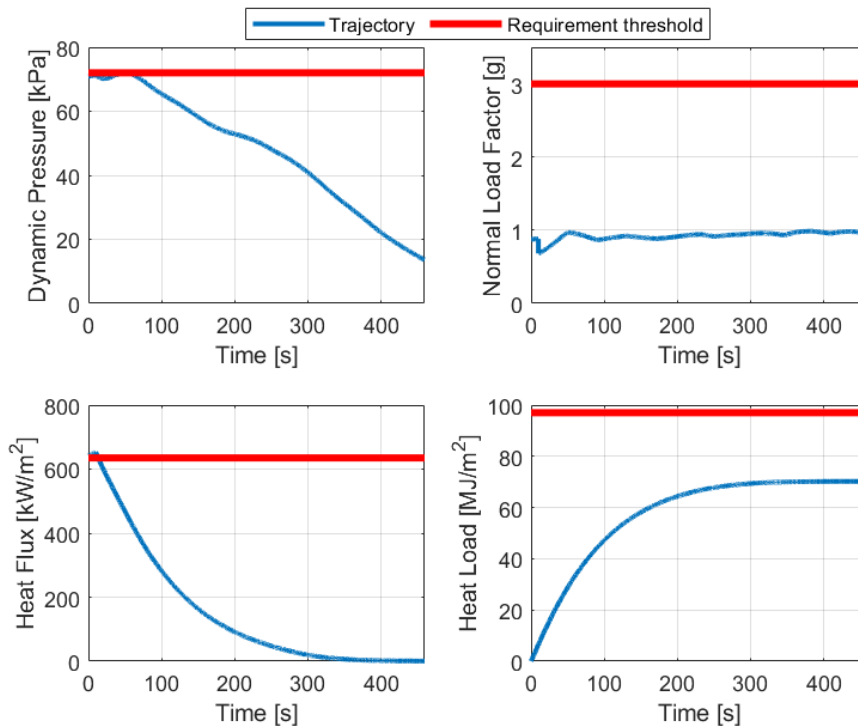


Figure 22: Mission parameters versus requirements: dynamic pressure (top left), normal load factor (top right), heat flux (bottom left) and heat load (bottom right)

## 6. Conclusions

This paper presents the first results achieved within the CIRA projects “SPACE-IPERSONICA-TEC” (funded by the national program PRORA) and “Research and Development of a hypersonic demonstrator” (co-funded by the Italian Aerospace Agency, ASI), having the common final goal of designing a hypersonic propelled demonstrator to increase the Technology Readiness Level of both system and technologies for future hypersonic transport vehicles.

First system activities, such as demonstrator configuration and mission scenario definition, aerodynamic database formulation, assessment of aero-propulsive balance, aerodynamic efficiency and preliminary nominal trajectory computation have been described in the paper.

The system PDR is foreseen in 2025.

## Acknowledgements

The work has been co-funded by Italian Space Agency and CIRA ScPA in the frame of the agreement nr. 2022-13-HH.0-F43D22000410005.

## References

- [1] J. Steelant et al., “Conceptual Design of the High-Speed Propelled Experimental Flight Test Vehicle HEXAFLY”, AIAA-2015-3539, 20th AIAA International Space Planes and Hypersonic Systems and Technologies Conference, Glasgow, Scotland, U.K., July 6-9, 2015.
- [2] Di Benedetto S., Di Donato M.P., Schettino A., Scigliano R., Nebula F., Morani G., Cristillo D., Marini M., Cardone S., Steelant J., Villace V., “The high speed experimental flight test vehicle of HEXAFLY INT: a multidisciplinary design”, CEAS Space Journal, published online on 5 January 2021, DOI: 10.1007/s12567-020-00341-5.
- [3] J. Steelant, R. Varvill, C. Walton, S. Defoort, K. Hannemann, M. Marini, “Achievements Obtained for Sustained Hypersonic Flight within the LAPCAT-II Project”, AIAA-2015-3677, 20th AIAA International Space Planes and Hypersonic Systems and Technologies Conference, July 06-09, 2015.

- [4] J. Steelant et al., “Achievements obtained within ATLLAS-II on Aero-Thermal Loaded Material Investigations for High-Speed Vehicles”, 21st AIAA International Space Planes and Hypersonics Technologies Conference, 6-9 March 2017, China.
- [5] Mack A., Steelant J., Adirim H., Lentsch A., Marini M., Pilz N., “FAST20XX: Achievements on European Suborbital Space Flight”, 7th European Symposium on Aerothermodynamics, Brugge, Belgium, May 2011.
- [6] Viola N., Fusaro R., Saracoglu B., Schram C., Grewe V., Martinez J., Marini M., Hernandez S., Lammers K., Vincent A., Hauglustaine D., Liebhardt B., Linke F., Fureby C., “Main Challenges and Goals of the H2020 STRATOFly Project”, *Aerotecnica Missili & Spazio* (2021) 100:95–110, Published online: 29 May 2021, <https://doi.org/10.1007/s42496-021-00082-6>.
- [7] Roncioni P., Vitagliano P. L., De Gregorio F., Pezzella G., Romano L., Paglia F., “Aerodynamic Appraisal of the VEGA-C Launcher”, *JSR-Journal of Spacecraft and Rockets*, 24 April 2023, <http://arc.aiaa.org> | DOI: 10.2514/1.A35610.
- [8] Viola N., Roncioni P., Gori O., Fusaro R., “Aerodynamic Characterization of Hypersonic Transportation Systems and Its Impact on Mission Analysis”, *MDPI-Energies*, 16 June 2021, <https://doi.org/10.3390/en14123580>.
- [9] System engineering general requirements, ECSS-E-ST-10C.
- [10] Technical requirements specification, ECSS-E-ST-10-06C.
- [11] S. Defoort, L. Serre, R. Grenon, Narmada, “ZEHST: Environmental challenges for hypersonic passenger transport”, AIAA 2012-5873, 18th AIAA/3AF International Space Planes and Hypersonic Systems and Technologies Conference, September 2012.
- [12] U. Mehta, M. Aftosmis, J. Bowles, S. Pandya, “SKYLON Aerodynamics and SABRE Plumes”, AIAA 2015-3605, 20th AIAA International Space Planes and Hypersonic Systems and Technologies Conference, Glasgow, Scotland, U.K., July 6-9, 2015.